Co-published by
Institute of Fluid-Flow Machinery
Polish Academy of Sciences
Committee on Thermodynamics and Combustion
Polish Academy of Sciences

Copyright©2026 by the Authors under licence CC BY-NC-ND 4.0

http://www.imp.gda.pl/archives-of-thermodynamics/

Experimental investigation of flow boiling heat transfer in a minichannel heat exchanger with countercurrent hot and cold fluid circuits

Kinga Strąk[a*], Dariusz Strąk[b]

[a]Kielce University of Technology, al. Tysiąclecia Państwa Polskiego 7, Kielce 25-314, Poland
[b]Independent Researcher, ul. Zagórska 72/1, Kielce 25-362, Poland
[*]Corresponding author email: kzietala@tu.kielce.pl

Received: 01.03.2026; revised: 12.06.2026; accepted: 30.06.2026

Abstract

This study presents a novel experimental investigation of flow boiling heat transfer in a minichannel module with simultaneous hot and cold fluid circuits. The novelty of the work lies in the analysis of a multilayer minichannel configuration with interacting hot and cold working fluids, enabling detailed evaluation of interfacial heat transfer mechanisms. Experiments were conducted in two groups of six parallel minichannels with rectangular cross-sections (1.5 mm depth, 20 mm width, and 140 mm length, hydraulic diameter 2.77 mm), heated by a 1000 W halogen lamp. The system was tested under steady laminar countercurrent flow conditions at a heat flux of 6000 W/m^2, with FC-72 fluid and distilled water mass flow rates of 0.006 kg/s and 0.0087 kg/s, respectively, and an inclination angle of 165°. The temperature of the outer copper plate surface was measured using an infrared camera. Local heat transfer coefficients were calculated using a one-dimensional computational approach at the heated plate – FC-72, FC-72 – central plate, central plate – water and water – closing plate interfaces. The results show the distributions of temperature and heat transfer coefficients along the channel length. An increase in the heat transfer coefficient was observed at the heated plate – FC-72 interface, whereas decreasing values were found at the remaining interfaces. The one-dimensional approach was validated using computational fluid dynamics simulations, showing a maximum discrepancy of 26.6% at the heated plate – FC-72 interface across all minichannels. These results offer insight into interfacial heat transfer in multilayer minichannel systems and support the design of compact, high-performance devices.

Keywords: Countercurrent flow; Flow boiling; Heat transfer coefficient; Minichannel; Working fluids

Vol. 47(2026), No. 3, 187–197; doi: 10.24425/ather.2026.7517

Cite this manuscript as: Strąk, K., & Strąk, D. (2026). Experimental investigation of flow boiling heat transfer in a minichannel heat exchanger with countercurrent hot and cold fluid circuits. *Archives of Thermodynamics*, 47(3), 187–197.

1. Introduction

Modern technological demands related to efficient thermal energy management and the intensification of heat transfer processes necessitate the optimisation of heat exchanger design. Small-sized heat exchangers represent a promising solution, as they provide a large heat transfer surface area while maintaining low mass and compact dimensions. Owing to their enhanced thermal efficiency and reduced size, such structures are widely used in electronic cooling systems, photovoltaic/thermal (PV/T) solar modules and server cooling applications. Advances in microchannel technology have led to the development of high-performance liquid-cooling devices that offer significantly higher heat transfer coefficients than conventional air-cooling systems and enabling further system miniaturisation.

The development of hybrid PV/T solar systems and the continuous improvement of their efficiency make effective thermal management a critical issue. Abdelrazik et al. [1] reviewed recent advances in PV/T technology, including various

Nomenclature

A – surface area, m^2
c_p – specific heat, J/(kg K)
d_h – hydraulic diameter, m
E – the radiation intensity for the copper heated plate, W/m^2
k – overall heat transfer coefficient, $W/(m^2 K)$
L – length of the minichannel, m
MRE – mean relative error
p – pressure, Pa
q – heat flux density, W/m^2
Q – heat flux, W
Q_m – mass flow rate, kg/s
Re – Reynolds number
T – temperature, K
x – coordinates in the direction of flow, m

Greek symbols

α – heat transfer coefficient, $W/(m^2 K)$
δ – thickness, depth, m
Δ – difference
ε – emissivity coefficient
λ – thermal conductivity, W/(m K)
ν – kinematic viscosity, m^2/s
ρ – density, kg/m^3
σ – surface tension, N/m

Subscripts and Superscripts

c – closing plate
Cu – copper plate
f – fluid
FC – FC-72 fluid
H – heated plate
in – inlet
IR – infrared camera
lin – linear
TC – thermocouple
out – outlet
s – ambient
w – distilled water

Abbreviations and Acronyms

AM – additive manufacturing
1D – one-dimensional
CFD – computational fluid dynamics
CHF – critical heat flux
GCI – grid convergence index
HTC – heat transfer coefficient
MCHS– microchannel heat sink
PCM – phase change material
PPMC– porous parallel minichannel
PV/T – photovoltaic/thermal
TIM – thermal interface material
VOF – volume of fluid

heat exchanger design solutions, and the application of nanofluids and phase change nanomaterials (nanoPCM) as alternatives to conventional cooling and thermal energy storage methods. The modified PV/T system reduced PV cell temperature by 13°C, increased electrical efficiency from 10.5% to 11.9%, and improved thermal efficiency by approximately 9% compared to a conventional PV/T system. These findings highlight the effectiveness of enhanced cooling and optimised heat collection techniques. In [2], Dubey and Tiwari presented a mathematical model for a flat-plate collector, and the calculated results were compared with experimental data. The study demonstrated a significant increase in instantaneous efficiency, from 33% to 64%, resulting from an increase in the glazing area.

During research on flow boiling heat transfer, systems in which the working fluid flows through multiple parallel channels of small dimensions are of particular importance, as they enable an increase in heat flux density while simultaneously reducing the volume of the heat exchanger, whether using mini- [3] or microchannels [3,4]. Kandlikar [3] highlighted the importance of the configuration of single- and multichannel heat exchangers in determining heat transfer and pressure drop. Flow boiling in mini- and microchannels is characterised by isolated bubble, slug and annular flow regimes. In microchannels, nucleating bubbles as small as 10–20 μm have been observed, while surface tension has been found to strongly influence flow behaviour. Significant pressure-drop fluctuations and flow reversals occur in multichannel evaporators. Heat transfer can be approximated using conventional flow boiling correlations; however, flow instabilities and pressure drop oscillations remain insufficiently understood. Small diameter evaporators generally operate with higher acceptable pressure drops to achieve enhanced heat transfer performance. The intensification of flow boiling is also influenced by the available heat transfer area, fluid stagnation zones, channel distribution and microchannel topology, as reported in the work of Lu et al. [4]. Optimisation of microchannel heat sink (MCHS) geometry significantly improves thermal performance. Biomimetic channel designs maintain temperature differences below 2°C, while ribbed microchannels enhance heat transfer by about 50% compared to smooth rectangular channels. Triangular/trapezoidal cross-sections and triangular cavity structures exhibit the best thermal characteristics. Additionally, diamond/copper composites and nanofluids are promising solutions for further heat transfer enhancement. Harirchian and Garimella [5] presented the characteristics of two-phase flow structures and the enhancement of flow boiling heat transfer of dielectric liquid FC-77 in parallel microchannels with widths ranging from 100 μm to 5850 μm. Experimental studies showed that channels of widths ≥ 400 μm exhibit conventional nucleate boiling over a wide range of heat fluxes. In contrast, smaller channels (< 400 μm) suppress wall bubble nucleation at relatively low heat fluxes, indicating a strong influence of channel size on flow boiling regimes and regime transitions. Mihai [6] discussed the analysis of the cooling process in micro- and nanochannels using a one-dimensional (1D) mathematical approach. The 1D approach simplifies analysis and is useful for determining effective heat transfer coefficients. The CPU cooling systems showed that efficient heat removal depends strongly on channel geometry and the thermal interface material (TIM). Microscope analyses revealed micro/nanochannels in the TIM with widths of 0.01–0.05 μm and depths up to 1000 Å, which

can disrupt heat transfer and contribute to overheating. Experimental studies also identified thermal expansion ('pump-out' effect) at the CPU–cooler interface, while surface roughness remained largely unchanged with increasing temperature, indicating good thermal stability of the TIM. Studies reported in the article by Prończuk and Krzanowska [7] on a shell-and-tube heat exchanger with a minichannel system of 0.8 mm internal diameter confirmed high heat transfer efficiency and highlighted the importance of precise pressure drop measurements. The transition from laminar to transitional flow was identified at a critical Reynolds number of Re = 1160. The authors developed a correlation for the tested heat exchanger, which showed good agreement with both the experimental data and correlations available in the literature. In contrast, Lan et al. [8] presented experimental studies of boiling heat transfer in a minichannel heat sink equipped with twisted tapes inducing swirling flow. The optimal configuration (twist ratio R = 3, tape length = 150 mm) reduced the wall superheat required for boiling onset by 34.4%, increased the heat transfer coefficient by up to 80.9%, and decreased inlet pressure fluctuations by 44.4% compared with a plain minichannel. Additionally, longer twisted tapes generated stronger swirl flow and more effective heat transfer enhancement. Ye et al. [9] presented studies on flow boiling heat transfer of R134a refrigerant in open minichannels, both ordinary and etched, at mass fluxes of 60.5–187.4 kg/(m^2 s) and heat fluxes up to 151 kW/m^2. The authors observed that surfaces with high nucleation site density exhibit the strongest hysteresis effect, leading to up to a 120% increase in the average heat transfer coefficient due to sequential activation of nucleation sites with increasing heat flux. Hysteresis is reduced in channels with limited nucleation sites or vapour backflow, and is influenced by inlet subcooling and mass flow rate. In the subsequent work, Yaghoubi et al. [10] analysed various geometric configurations of channels with rectangular side-wall cavities to enhance the R141b flow boiling heat transfer. The introduction of these cavities led to a six-fold increase in the heat transfer coefficient compared to a plain channel. The cavities act as nucleation sites, reducing the onset of boiling and enhancing heat transfer in bubbly flow. However, in slug flow and near outlet regions, they may reduce HTC (heat transfer coefficient) due to higher wall temperatures. Ye et al. [11] investigated minichannels produced by additive manufacturing (AM) with microengineered surfaces for R134a flow boiling. These channels achieved a 210% increase in heat transfer coefficient compared to conventionally machined channels, achieving values up to 54.9 kW/(m^2 K). Enhancement factors reached 2.5–3.0, confirming that engineered microstructures provide abundant nucleation sites and significantly improve boiling heat transfer performance. Another type of surface enhancement was applied in integrated server cooling circuits during HFE-7100 flow boiling by Shang et al. [12]. Radiators made of 6061 aluminium alloy with a hydraulic diameter of 2 mm were used, where etching created a porous parallel minichannel (PPMC) structure. Such porous surfaces acted as effective nucleation sites and significantly reduced wall temperature (the maximum wall-temperature reduction reached 2.39% at 181.4 kg/(m^2 s) and ~70 kW/m^2) during flow boiling. Titanium carbide nanowires with thicknesses of 4 μm and 12 μm were also employed to intensify flow boiling by Sun et al. [13]. The results showed that a nanowire surface of 12 μm thickness increased the heat transfer coefficient by 19.84% under single-phase flow, whereas a 4 μm nanowire surface increased the coefficient by 27.9% under two-phase flow conditions. Li et al. [14] examined flow stability during boiling in minichannels with phase-separated configurations using porous membranes for vapour–liquid separation. In tests with multiple-pore, phase-separated configurations, a 24.71% reduction in pressure drop was observed in two-phase flow compared to conventional poreless structures. Hsu et al. [15] employed minitubes with diameters of 30 mm and 10 mm, featuring hydrophilic and hydrophobic surfaces, to enhance thermal efficiency during flow boiling. The results showed that hydrophilic surfaces (5° contact angle) significantly improved heat transfer performance, while hydrophobic surfaces (150° contact angle) stabilised the vapour layer, reducing overall pressure drop to 698.4 Pa and minimising fluctuations.

Comprehensive reviews of the literature on heat transfer have been presented in studies [16,17]. Pereira et al. [16] summarised active pool-boiling enhancement techniques beyond surface modification, including fluid additives, external fields, mechanical interventions and thermal-geometric optimisation. These methods aim to improve the heat transfer coefficient, increase critical heat flux (CHF), and reduce boiling hysteresis. The review also highlights the lack of comprehensive datasets and standardised reporting, which limits the development of predictive models and practical cooling system designs. Etminan et al. [17] examined gas-liquid and liquid-liquid two-phase flows in microchannels, focusing on flow-regime transitions, liquid-film behaviour and pressure drop characteristics. The authors highlighted the lack of a universal flow-regime classification and emphasised the key role of liquid-film thickness and contact angle in determining flow patterns, pressure drop, and heat and mass transfer. Existing correlations for slug length, film thickness, and pressure drop are based on dimensionless numbers, flow rate ratios and thermophysical properties.

In the previous study [18], a comparison between one-dimensional and two-dimensional approaches for estimating the heat transfer coefficient was performed using the Trefftz method. The analysis was based on energy equations for the copper plate and FC-72, supported by appropriate boundary conditions. Experiments were conducted on a test module with two rectangular minichannels (1.5 mm×24 mm×240 mm). Although heat transfer in minichannel systems has been widely studied, few works combine infrared heat flux measurements with CFD (computational fluid dynamics) validation for separate hot and cold channel groups. In this study, the heat transfer coefficient was determined experimentally for 12 minichannels (six hot and six cold) using a 1D approach and validated based on STAR-CCM+ simulations under countercurrent flow conditions [19].

The available data for the considered configuration remain limited in the literature, which highlights the need for dedicated experimental and numerical analysis. The main novelties of this study include: (i) a redesigned test module with two groups of minichannels and copper plates replacing previous materials (e.g. glass, solar cells, Haynes-230), (ii) channel dimensions of

140 mm×20 mm×1.5 mm (d_h = 2.77 mm), (iii) heating of a copper plate using a 1000 W halogen lamp, (iv) experiments at heat flux of 6000 W/m^2 under countercurrent flow conditions at the hot channel ($Q_{m,FC}$ = 0.006 kg/s), cold channel ($Q_{m,W}$ = 0.0087 kg/s), and a 165° inclination, and (v) combined experimental, 1D analytical and CFD analysis of FC-72 refrigerant and distilled water flow in a steady-state multi-minichannel system.

This paper presents innovative experimental studies on flow boiling heat transfer of two working fluids: FC-72 in the hot minichannel circuit and distilled water in the cold minichannel circuit under subcooled boiling conditions. Temperature distributions of the copper heated plate, the central copper plate, and the working fluids were measured at the inlets and outlets of both minichannel circuits. Local heat transfer coefficients at the interfaces between each partition of the working fluid plate were calculated using a one-dimensional computational approach based on the experimental data. Previous studies on flow boiling in minichannels have predominantly focused on heat exchangers with a single working fluid circuit. However, data on the heat transfer coefficients of individual partitions, as well as studies employing minichannel arrays with two fluid circuits (additionally cooled with water), are lacking. The presented test module, featuring two countercurrent fluid circuits, has potential applications in cooling systems for high-performance computer processors.

2. Research stand and research procedure

2.1. Research stand

Figure 1 shows a schematic of the test rig with its main components. The experimental setup comprises a test module with a group of minichannels (1), magnetic circulation pumps (2a,2b), pressure transmitter (3), heat exchangers (4a,4b), filters (5a,5b), electromagnetic flow metres (6a,6b) and air separators (7a,7b). The primary flow circuits consist of two closed circulation loops for the working fluids: a low-boiling refrigerant FC-72 circuit (referred to as 'hot') and a distilled water circuit (referred to as 'cold'). The output of magnetic circulation pumps (type GZD.Q57.JDS-B380 (BLDC), MICROPUMP INC., USA) was regulated using three-phase electric inverters. The main components of the measurement data acquisition system include an infrared camera (8), a data acquisition station (9), and a personal computer (10). The heat source for the copper heated plate consisted of two halogen lamps (11), and the illuminance on the heated plate was measured using a luxmeter (12).

The key component of the test rig is the test module containing a group of rectangular minichannels (1), which share a common wall. This wall is a central copper plate with a thickness of 0.5 mm. The dimensions of a single minichannel (from each of the two groups of six minichannels) are 1.5 mm in depth, 20 mm in width, and 140 mm in length.

The outer walls of minichannels are formed by copper plates: a 3 mm thick heated plate and an outer plate, referred to as the module 'closing' plate, with a thickness of 0.5 mm.

Figure 2 shows the characteristic dimensions of the test module.

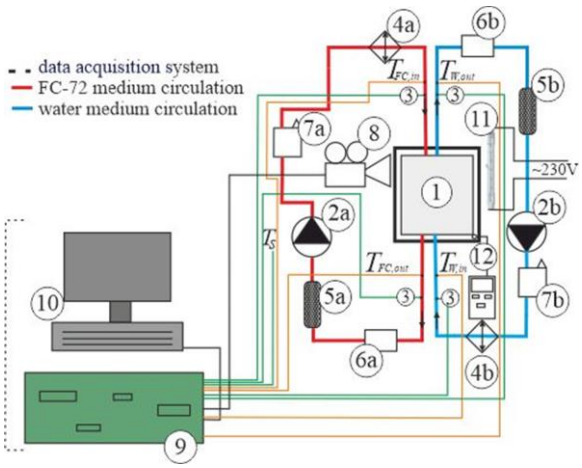


Fig. 1. Schematic of the test rig and its main components: 1 – test module, 2a, 2b – magnetic circulation pump, 3 – pressure transmitter, 4a, 4b – heat exchanger, 5a, 5b – filter, 6a, 6b–- electromagnetic flowmeter, 7a, 7b – air separator, 8 – infrared camera, 9 – data acquisition station, 10 – personal computer, 11 – halogen lamp, 12 – luxmeter.

In one group of six minichannels (referred to as 'hot'), the FC-72 refrigerant flows, and its outer wall is heated by halogen lamps (11 in Fig. 1). In the second group of six minichannels (referred to as 'cold'), distilled water flows in the countercurrent direction. After exiting the channels, both working fluids are cooled with tap water via heat exchangers (4a and 4b in Fig. 1).

The temperature of the heated outer surface of the copper plate was measured using a Flir E60 infrared camera. This surface, which is in direct contact with the surrounding environment, was coated with a thin layer of black paint with a known emissivity of 0.97. The temperature of the central copper plate was measured point-wise at its ends on the side where the FC-72 fluid flows, using K-type thermocouples. The temperatures of the working fluids (measured with K-type thermocouples) and the pressures (measured with pressure transmitters)

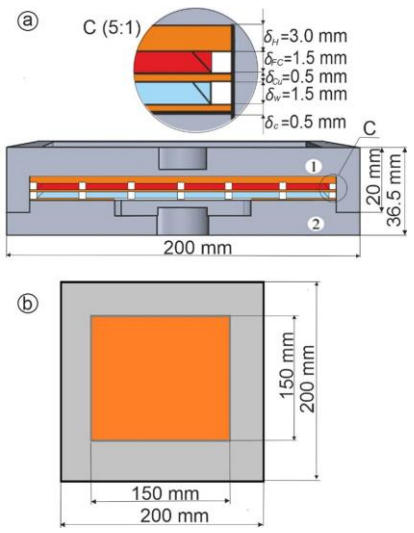


Fig. 2. Characteristic dimensions of the test module: a) cross section, b) view from the heated plate side.

were recorded at the inlet and outlet of each minichannel group.

Figure 3 shows views of the test rig and its main components. The basic physicochemical properties of the low-boiling FC-72 refrigerant and distilled water are summarised in Table 1. The specifications of the main components of the experimental apparatus, along with the maximum measurement errors, are provided in Table 2 and in [18,20,21].

2.2. Research procedure

Prior to the main experimental investigations, several working fluids, including HFE-649 and FC-72, were examined in the hot channel. FC-72 was ultimately selected owing to its higher boiling point, enhanced flow stability and greater volumetric heat capacity. An optimal channel configuration was subsequently defined, consisting of minichannels with a hydraulic diameter below 3 mm, with the channels distributed over the entire active area of the module. The working fluid flow rates were adjusted to ensure uniform coolant distribution across all channels and to achieve appropriate pressure conditions within the system. The higher the mass flow rates of the working fluids in both circuits, the greater the amount of heat removed from the solar cell, resulting in a reduction of the cell temperature. The imposed heat flux was specified to be representative of realistic operating conditions of the collector. An inclination angle of 165° was identified as optimal, representing a minor departure from the horizontal configuration. Optimisation-related issues can be found in the literature [22–24].

After degassing the two flow circuits (hot and cold) and stabilising the pressures and fluid flow rates, the heat flux supplied to the copper heated plate was gradually increased using two

Table 1. Basic physicochemical properties of the FC-72 refrigerant and distilled water.

Properties of the working fluids	FC-72 refrigerant	Distilled water
Boiling point temperature (K)	329	373
Critical temperature (K)	722	647
Kinematic viscosity (m^2/s)	0.38×10^3	1.00×10^3
Density (kg/m^3)	1680.0	998.2
Vapour pressure (Pa)	30.9×10^3	2.3×10^3
Specific heat (J/(kg K))	1100	4187
Thermal conductivity (W/(m·K))	0.057	0.591
Surface tension (N/m)	0.01	0.06

Table 2. Basic data of control and measurement equipment and sensors.

Parameter	Apparatus/ Measuring sensor	Type/ Model, Manufacturer	Measuring range	Measurement error
Heated plate temperature	Infrared camera	E60, Flir	20 – 120°C 0 – 650°C	±1 °C or ±1% in the range 0–120°C*
Temperature at the inlet/ outlet of FC-72 and distilled water; ambient temperature	Thermocouples	Type K (221 b), Czaki Thermo-Product	–40 – 375°C	1.5°C in the range –40–375°C*
Pressure at the channel inlet/ outlet, atmospheric pressure	Pressure transmitter	A-10, Wika	0 – 2.5 bar	0.5% of full scale*
Mass flow rate of fluids	Electromagnetic mass flowmeter	SM6004, IFM	6 – 1500 kg/s	±0.2% of reading*
Light intensity	Luxmeter	OHM-HD2102.1, Delta	0 – 1999.9 W/m^2	±0.02 W/m^2 or ± 2%*

*According to the manufacturer's specifications.

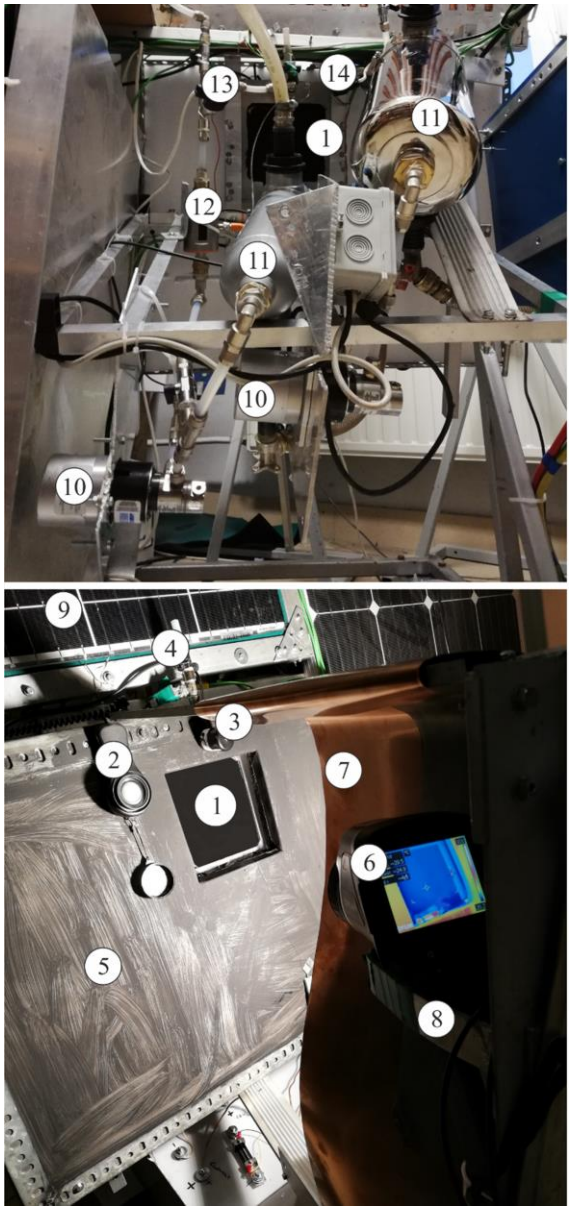


Fig. 3. Views of the test rig and its main components at the test module position angled 165° from the horizontal: 1 – test module, 2 – luxmeter, 3 – luxmeter probe, 4 – hot circuit vent valve, 5 – aluminium heat shield, 6 – infrared camera, 7 – copper heat shield, 8 – infrared camera mounting bracket, 9 – solar panel, 10 – magnetic circulation pump, 11 – heat exchangers, 12 – electromagnetic flowmeter, 13 and 14 – pressure transducers.

halogen lamps. The lamps had a total power of 2000 W and were positioned 330 mm from the surface of the heated plate, at a 90° angle. The infrared (IR) camera was positioned at a 30° angle on the thermal shield on the left side of the test module. The experiments were conducted under steady-state conditions for 3 min at various heat flux densities. Due to the extensive dataset obtained, the results presented herein are limited to a representative case corresponding to a single heat flux density and the thermal and flow parameters listed in Table 3.

Experimental data were recorded using DaqView software (version 9.1.35) in conjunction with the data acquisition station. Data corresponding to a heat flux density of 6000 W/m^2 applied to the heated plate surface were selected for detailed analysis. All tests were performed with a constant mass flow rate in both minichannel circuits (hot, $Q_{m,FC}$ = 0.006 kg/s, and cold, $Q_{m,w}$ = 0.0087 kg/s) under laminar flow conditions with a slight overpressure (see Table 3).

Table 3. Experimental parameters and their ranges of variation.

Experimental parameters	Range of variation
FC-72 refrigerant temperature, T_{FC} (K)	298.46–300.95
Distilled water temperature, T_W (K)	290.45–291.95
Surface temperature of the copper heated plate, $T_{H,IR}$ (K)	299.75–306.95
Temperature of the copper plate central to the minichannels, T_{Cu} (K)	290.65–291.65
Inlet pressure to the hot minichannel, p_{in} (kPa)	110–116
Inlet pressure to the cold minichannel, p_{out} (kPa)	99.1–104
Mass flow rate for the hot channel, $Q_{m,FC}$ (kg/s)	0.006
Mass flow rate for the cold channel, $Q_{m,W}$ (kg/s)	0.0087
Heat flux density, q (kW/m²)	6

Throughout each experimental series, subcooled liquid entered the minichannels and was heated as it flowed along the heated wall toward the outlet. The heat flux applied to the heated surface of the minichannel was gradually increased during the experiments. Consequently, the heat transfer regime evolved from single-phase forced convection at the lowest heat flux densities to subcooled flow boiling at higher heat flux levels. In the subcooled boiling regime, the fluid layer adjacent to the heated surface reached locally superheated conditions, whereas the bulk liquid remained subcooled. As a result, a two-phase liquid–vapour mixture was formed near the channel outlet and subsequently directed to an auxiliary heat exchanger (condenser), where the vapour phase was condensed.

Due to the design of the heat exchanger integrated with the photovoltaic (PV) panel, direct observation of the two-phase flow structures was not feasible. Consequently, the identification of boiling flow regimes was limited to inferences based on the available experimental data, and only the flow regimes likely to occur within the exchanger could be considered.

3. One-dimensional approach

This paper proposes a simplified one-dimensional (1D) computational approach, which considers heat flow in a single direction, perpendicular to both the fluid flow and the width of the minichannel. A linear temperature distribution along the minichannel is assumed under steady-state heat transfer through a flat wall, with only one direction of heat flow considered (perpendicular to the fluid flow and the minichannel width). Heat losses along the channel axis are assumed negligible, no internal heat sources are present, and the thermal conductivity is considered constant. To provide clarification, the heat flux is indicative of the conductive heat flux within the copper heated plate, as determined by the surface's IR measurement. In our experiment, the copper plate (156 mm × 156 mm) was coated with a high-emissivity paint (ε = 0.97), and the measured radiation intensity from the heated plate was E_{IR} = 6000 W/m^2. The heat flux density was then estimated using the methodology presented in [19]:

$$q \approx \frac{E_{IR}}{\varepsilon}, \tag{1}$$

where: E_{IR} – radiation intensity of the copper heated plate, ε – emissivity coefficient.

The heat transfer coefficient α_1 at the interface between the copper heated plate and the FC-72 refrigerant was determined based on the known temperature distribution of the outer surface of the heated plate, following the methodology of [18,20,21,25]:

$$\alpha_1(x) = \frac{q\lambda_H}{\lambda_H(T_{H,IR}(x) - T_{FC,lin}(x) - q\,\delta_H)}, \tag{2}$$

where: δ_H – thickness of the heated plate, λ_H – thermal conductivity of the heated plate, $T_{H,IR}(x)$ – surface temperature of the heated plate, $T_{FC,lin}(x)$ – the temperature of the FC-72 refrigerant, assumed to vary linearly from the inlet to the outlet of the minichannel, x – the distance from the minichannel inlet.

The heat transfer coefficient α_2 at the interface between the FC-72 refrigerant and the central copper plate was estimated using the formula, as in [18,20,21,25]:

$$\alpha_2(x) = \frac{Q_{m,FC}c_{p,FC}(T_{FC,in} - T_{FC,out})}{A(T_{FC,lin(x)} - T_{Cu,lin(x)})}, \tag{3}$$

where: A – surface area of the central plate, $Q_{m,FC}$ – mass flow rate of the FC-72 refrigerant, $c_{p,FC}$ – specific heat of FC-72, $T_{Cu,lin}(x)$ – temperature of the central copper plate approximated linearly based on the known temperature recorded by two K-type thermocouples ($T_{TC,1}$, $T_{TC,2}$) located at the ends of the side of the copper plate on the FC-72 refrigerant side.

Figure 4 shows a general schematic of the test module with minichannels, illustrating the adopted 1D approach for countercurrent flow.

To determine the heat transfer coefficient at the interface between the central copper plate and distilled water, the relationship for the overall heat transfer coefficient (k) was used:

$$\frac{1}{k} = \frac{1}{\alpha_1(x)} + \frac{1}{\alpha_2(x)} + \frac{\delta_{Cu}}{\lambda_{Cu}} + \frac{1}{\alpha_3(x)}, \tag{4}$$

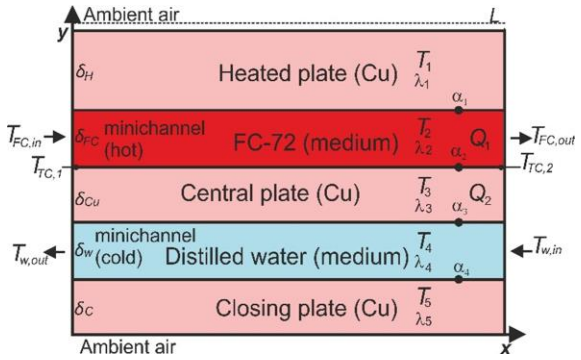


Fig. 4. General schematic of the test module with minichannels, illustrating the one-dimensional approach for countercurrent flow.

where δ_{Cu} is the central plate thickness and λ_{Cu} is the thermal conductivity of the central plate. The overall heat transfer coefficient was calculated for countercurrent flow, similarly to [19,26]:

$$k = \frac{Q_{FC}+Q_w}{2A\,\Delta T}, \tag{5}$$

where ΔT denotes the logarithmic mean temperature difference of the liquids, and Q stands for the heat flux transferred to/from the medium. The heat transfer coefficient α_3 at the interface between the central copper plate and the distilled water was determined according to the methodology applied in [19–21]:

$$\alpha_3(x) = \left[\frac{1}{k} - \frac{1}{\alpha_1(x)} - \frac{1}{\alpha_2(x)} - \delta_{Cu}\frac{1}{\lambda_{Cu}}\right]^{-1}. \tag{6}$$

Finally, the heat transfer coefficient α_4 at the distilled water–copper plate was estimated, following the procedures presented in [19,21]:

$$\alpha_4(x) = -\left[\frac{1}{\alpha_1(x)} + \frac{1}{\alpha_2(x)} + \delta_{Cu}\frac{1}{\lambda_{Cu}} - \frac{1}{k} + \frac{1}{\alpha_3(x)}\right]^{-1}. \tag{7}$$

The mean relative error (MRE) of the heat transfer coefficient α_1 (at the interface between the copper heated plate and the FC-72 refrigerant) using a one-dimensional approach was determined from the formula [18]:

$$\mathrm{MRE} = \sqrt{\begin{array}{c}\left(\frac{\partial\alpha(x)}{\partial q}\Delta q\right)^2 + \left(\frac{\partial\alpha(x)}{\partial T_{H,IR}}\Delta T_{H,IR}(x)\right)^2 + \\ + \left(\frac{\partial\alpha(x)}{\partial T_{FC,l_in}}\Delta T_{FC,l_in}(x)\right)^2 + \left(\frac{\partial\alpha(x)}{\partial T_{\lambda_H}}\Delta\lambda_H\right)^2 + \left(\frac{\partial\alpha(x)}{\partial T_{\lambda_H}}\Delta\delta_H\right)^2\end{array}}. \tag{8}$$

Furthermore, the individual contributions to the mean relative error of the calculated heat transfer coefficient are presented below:

- heated plate surface temperature measured by an IR camera, $\Delta T_{H,IR}(x)$ = 1.0 K;
- fluid temperature measured by a thermocouple, $\Delta T_{FC,lin}(x)$ = 0.34 K;
- thermal conductivity of the heated plate $\Delta\lambda_H$ = 0.1 W/(m·K);
- thickness of the heated plate, $\Delta\delta_H = 5\times10^{-5}$ m.

The estimated total measurement error was 2% for the heat flux density (q), and the mean relative error was 14.53% for the heat transfer coefficient (MRE).

The mean relative errors in the 1D approach were low and showed decreasing values with increasing heat flux supplied to the heated plate. As reported by Piasecka et al. [18], the maximum mean relative error of the heat transfer coefficient was 12.93% and occurred at the lowest applied heat flux density q = 12.26 kW/m^2. For the same operating conditions, the mean relative error associated with the heat flux density was significantly lower, reaching only 1.41%.

4. Results

4.1. Results of one-dimensional approach

Based on the experimental data, the surface temperature of the copper heated plate was analysed under laboratory conditions at an ambient temperature of 26°C, a relative humidity of 34% and an atmospheric pressure of 1017 hPa. A luxmeter was used to measure the illuminance on the surface of the heated plate.

Figure 5 shows a thermogram of the outer surface of the copper heated plate, captured using a Flir E60 infrared camera, for a heat flux density of 6000 W/m^2, with the test module inclined at 165° to the horizontal. The six lines marked in the figure (#1 to #6) correspond to the central axes of each of the six minichannels.

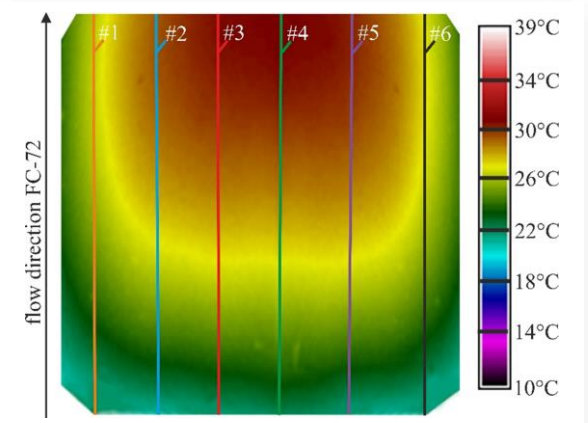


Fig. 5. Thermogram of the copper heated plate surface obtained from a Flir E60 infrared camera for a heat flux density of 6000 W/m^2, module orientation 165°.

On the outer surface of the copper heated plate, the highest temperature was recorded at the outlet section (33.8°C), while the lowest temperature (19.4°C) was observed near the inlet of the minichannels. The temperature distribution across the individual layers of the module, as a function of the distance from the minichannel inlet for the six channels (#1 to #6), is presented in Figs. 6 and 7.

The temperature of the individual layers of the module increased with the distance from the minichannel inlet. The highest temperatures on the surface of the copper heated plate were observed in the centrally located channels (Fig. 6a, channels #3 and #4), reaching approximately 33.8°C, while the lowest temperatures occurred near the side walls (Fig. 6a, channel #1). In the FC-72 minichannels (Fig. 6b), on the central copper plate

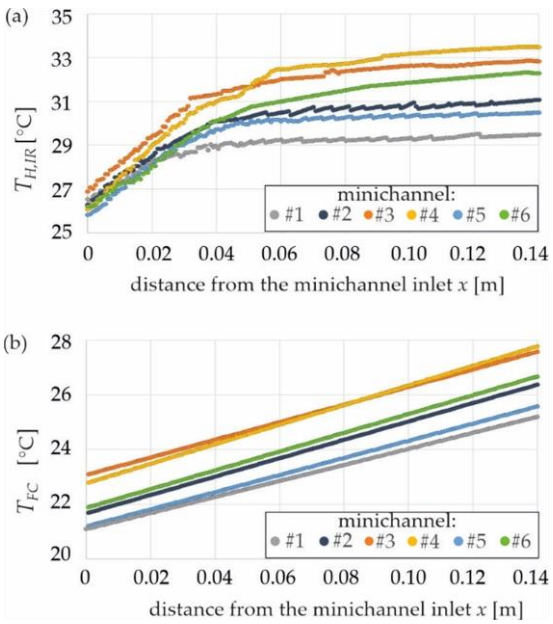


Fig. 6. Temperature distribution across the individual layers of the module as a function of distance from the minichannel inlet for six channels (marked #1 to #6): (a) on the surface of the heated plate, and (b) within the minichannels with FC-72 refrigerant.

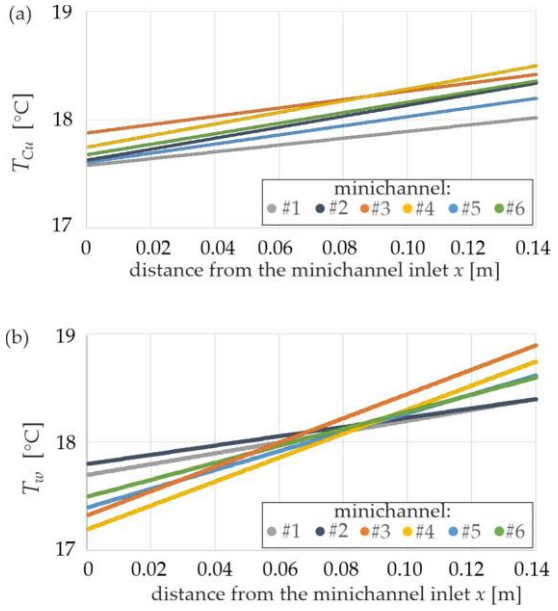


Fig. 7. Temperature distribution across the individual layers of the module as a function of distance from the minichannel inlet for six channels (marked #1 to #6): (a) on the central plate, and (b) within the minichannels with distilled water.

(Fig. 7a) and in the distilled water minichannels (Fig. 7b), the temperature increased approximately linearly with the distance from the channel inlet. The highest temperatures were consistently observed in the central channels (Figs. 6b and 7, channels #3 and #4), with maximum values of 27.8°C (Fig. 6b), 18.4°C (Fig. 7a), and 18.7°C (Fig. 7b).

Figures 8 and 9 present the distributions of local heat transfer coefficients as a function of the distance from the minichannel inlet for a selected heat flux density, corresponding to the experimental parameters listed in Table 3. The coefficients were calculated using the proposed one-dimensional computational approach at the interfaces of the individual layers:

- copper heated plate – FC-72 refrigerant (Fig. 8a),
- FC-72 refrigerant – central copper plate (Fig. 8b),
- central copper plate – distilled water (Fig. 9a),
- distilled water – closing copper plate (Fig. 9b).

The local heat transfer coefficient α_1 at the interface between the copper heated plate and the FC-72 refrigerant exhibited increasing values from one-third of the distance from the inlet toward the channel outlet. The highest value, 1.6 kW/(m^2 K), was observed at the channel outlet near the side walls (Fig. 8a, channel #1), corresponding to the location where the lowest temperature was recorded (Fig. 6a). The remaining coefficients from α_2 to α_4, representing the interfaces FC-72 refrigerant – central copper plate, central copper plate – distilled water, and distilled water – closing plate, respectively, showed decreasing values from the inlet to the outlet of the minichannel. This behaviour is likely related to an increase in the local temperature of the central plate in this region. The highest values of heat transfer coefficients at the channel entrances were approximately 1.55 kW/(m^2 K) (Fig. 8, channels #2, #4 and #6), while a maximum of 1.58 kW/(m^2 K) was obtained at the channel exit (Fig. 8a, channel #1).

Halogen lamps generate a heat flux that unevenly heats the upper surface of the copper plate (Fig. 5). Copper, as a material with high thermal conductivity (400 W/(m·K)), effectively distributes heat throughout the entire surface of the heated plate. In the vicinity of the central channels (Fig. 5, channels #3 and #4), local overheating of the heated plate wall occurs.

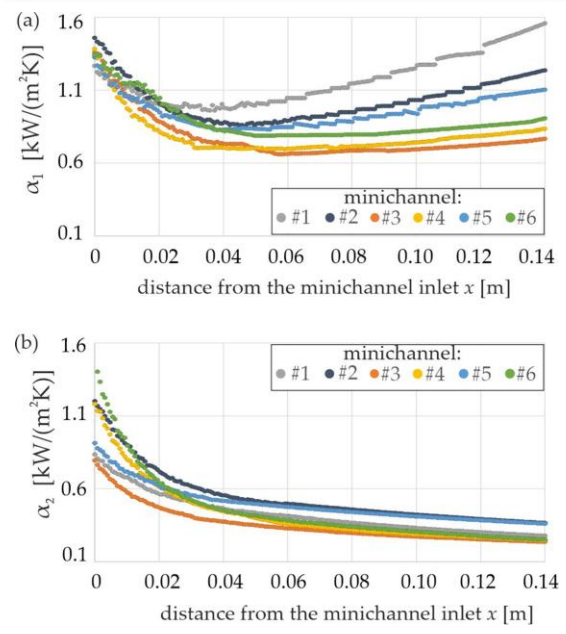


Fig. 8. Heat transfer coefficient as a function of distance from the minichannel inlet for six channels (marked #1 to #6) determined using the 1D approach at the interfaces: a) copper heated plate – FC-72 refrigerant, b) FC-72 refrigerant – copper central plate; heat flux density 6000 W/m^2, module inclined at 165°.

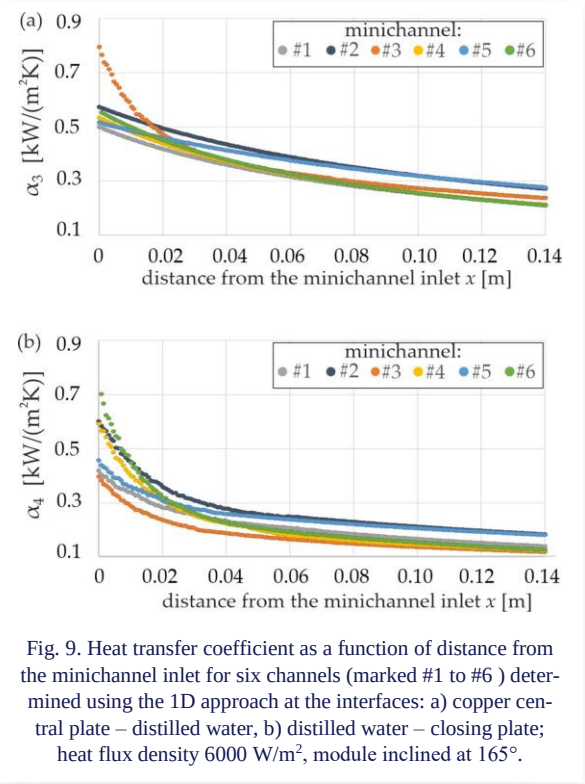


Fig. 9. Heat transfer coefficient as a function of distance from the minichannel inlet for six channels (marked #1 to #6) determined using the 1D approach at the interfaces: a) copper central plate – distilled water, b) distilled water – closing plate; heat flux density 6000 W/m^2, module inclined at 165°.

The FC-72 refrigerant, characterised by a low boiling point, undergoes intense heating already at the channel inlet, particularly in the central minichannels, where local subcooled boiling occurs. In these central channels (Fig. 5, channels #3 and #4), the onset of subcooled boiling is observed in the outlet sections, accompanied by an increase in the heat transfer coefficient α_1, reaching values of 0.8–1.6 kW/(m^2 K), and a corresponding rise in temperature toward the channel outlet.

Minichannels near the side walls (Fig. 6a, #1 and #5) exhibit lower surface temperatures on the heated plate, yet they present the highest local values of α_1 at the interface between the heated plate and the FC-72 refrigerant (Fig. 8a). The countercurrent flow of the working fluids amplifies the local temperature difference in the central plate, further enhancing the heat transfer process.

The central copper plate serves as a thermal bridge between the two working fluid circuits, maintaining an average temperature of approximately 18.5°C (Fig. 7a). Distilled water acts as the cooling medium, removing heat from the central plate. In this closed system, subcooled boiling occurs on the FC-72 side of the central plate, while forced single-phase convection dominates on the water side.

The local subcooled boiling may have occurred at the channel walls, particularly within the adjacent near-wall boundary layer. The liquid in the vicinity of the heated surface reached a superheated state, whereas the bulk fluid remained subcooled (in the hot minichannel with FC-72). In the cold minichannel, heat transfer was governed exclusively by single-phase convection, leading to low temperature gradients between the channel wall and the distilled water.

Consistent with findings reported in the literature [28] for flow boiling in small channels, forced convection boiling is primarily governed by mass flux and vapour quality, whereas nucleate boiling is mainly influenced by heat flux and saturation pressure. Furthermore, nucleate boiling was identified as the dominant heat transfer mechanism throughout the investigated heat flux range.

4.2. Validation of the proposed 1D approach against STAR-CCM+ simulations

The experimental results were validated through comparison with the corresponding CFD predictions. Numerical simulations were conducted using Simcenter STAR-CCM+ (version 2020.2.1, Build 15.04.010) on a workstation equipped with two Intel Xeon E5-2698v4 processors (40 cores total, 3.6 GHz) and 128 GB of RAM. Additionally, the quality of the computational meshes used in the numerical analysis was assessed. Mesh convergence and discretisation errors were evaluated using the grid convergence index (GCI) method, following the procedure and boundary conditions described in [19]. A multiphase volume of fluid (VOF) model was employed to simulate the flow of immiscible fluids and track the phase interface. The governing equations for fluid flow and heat transfer were adopted from [19]. Mesh quality was assessed using the GCI method for three base mesh sizes (2, 3 and 5 mm). The obtained GCI values (0.14% for the fine mesh and 0.35% for the coarse mesh) confirmed mesh convergence and solution reliability. Therefore, the 5 mm mesh was adopted for subsequent simulations, with an estimated discretisation error below 1%.

A comparison of the heat transfer coefficient values obtained using the 1D approach and STAR-CCM+ simulations was conducted for a representative case, involving the heat transfer coefficient α_1 (at the interface between the copper heated plate and the FC-72 refrigerant), at a heat flux density of 6000 W/m^2. Figure 10 shows the maximum relative differences between α_1 values calculated using Eq. (2) and the corresponding values determined from STAR-CCM+ simulations. The results indicate that the highest maximum relative differences in the heat transfer coefficient were observed for minichannels #3 and #6, reaching 30%, whereas the lowest value was recorded for minichannel #1 (19.5%). Furthermore, the average of the maximum relative differences across all minichannels was found to be 26.6%.

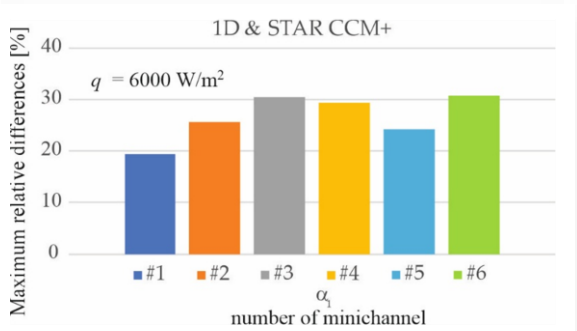


Fig. 10. Maximum relative differences between the values of heat transfer coefficient α_1, calculated using Eq. (2) and those obtained from STAR-CCM+ simulations, based on the average across all minichannels at a heat flux density of 6000 W/m^2.

The heat transfer coefficient at the interface between the heated copper plate and the FC-72 refrigerant (α_1) exhibited the highest maximum relative differences compared to the other calculated heat transfer coefficients ($\alpha_2 - \alpha_4$). Similar values were reported in a previous study [19], where the highest maximum relative difference was also observed for α_1 at a medium heat flux density of 2000 W/m^2, reaching 35.7%. These discrepancies can be attributed primarily to the limitations of the one-dimensional approach, which relies on spatially averaged parameters and does not capture local variations in velocity and temperature fields within the near-wall region. In contrast, the CFD approach resolves three-dimensional flow structures, including boundary layer development and local thermal non-uniformities, which play a significant role in heat transfer within minichannels.

An additional source of discrepancy may be the occurrence of localised subcooled boiling in the hot minichannel, which can enhance heat transfer through intermittent bubble nucleation and collapse. Such phenomena are not represented in the 1D approach. Nevertheless, the cold minichannel remains within the single-phase forced convection regime.

Further discrepancies may also arise from model idealisations, including the simplified treatment of inlet and outlet regions, neglect of surface roughness, manufacturing tolerances and local flow non-uniformities. Moreover, the CFD simulations assumed idealised thermophysical properties and steady-state operating conditions, whereas the experimental system may experience local fluctuations and unavoidable external heat losses.

A grid independence study confirmed mesh adequacy, with variations below 1%. CFD results were extracted along the channel centreline to ensure direct comparison with the 1D approach and experimental data.

The present findings are in agreement with results reported by other authors [28], confirming that channel geometry and flow arrangement strongly influence fluid flow and heat transfer in minichannel systems. The referenced study combined experimental measurements with CFD simulations to investigate fluid flow in mini cooling channels.

5. Conclusions

The main conclusions of this study can be summarised as follows:

- Experimental investigations were conducted on a countercurrent minichannel heat exchanger consisting of two groups of six rectangular minichannels carrying FC-72 refrigerant and distilled water. A heat flux density of 6000 W/m^2 was supplied to the heated copper wall. The test module consisted of twelve parallel rectangular minichannels, separated by a central copper plate, and inclined at 165° to the horizontal.
- A simplified one-dimensional approach was developed to determine local heat transfer coefficients at the interfaces: the copper heated plate – FC-72 refrigerant, FC-72 refrigerant – central copper plate, central copper plate – distilled water, and distilled water – closing plate.
- The results demonstrated a progressive increase in temperature along the flow direction in all regions of the heat exchanger. The local heat transfer coefficient increased at the heated plate – FC-72 interface and decreased at the remaining interfaces along the heat transfer path.
- The results indicate the likely occurrence of local subcooled boiling in the FC-72 minichannels, while heat transfer in the water minichannels remained within the single-phase forced convection regime.
- Validation of the one-dimensional approach against CFD simulations showed satisfactory agreement (average discrepancy of 26.6% across all analysed minichannels). The observed differences were mainly associated with model simplifications and local flow and heat transfer phenomena that cannot be fully represented by the one-dimensional approach.
- The application of a copper heated plate ensured effective heat spreading within the module, while the use of parallel minichannels increased the heat transfer area and intensified heat exchange processes.
- The proposed heat exchanger configuration shows potential for thermal management systems and photovoltaic–thermal applications, where efficient cooling and heat recovery are required.

References

[1] Abdelrazik, A.S., Al-Sulaiman, F.A., Saidur, R., & Ben-Mansour, R. (2018). A review on recent development for the design and packaging of hybrid photovoltaic/thermal (PV/T) solar systems. *Renewable and Sustainable Energy Reviews*, 95(C), 110–129. doi: 10.1016/j.rser.2018.07.013

[2] Dubey, S., & Tiwari, G.N. (2008). Thermal modeling of a combined system of photovoltaic thermal (PV/T) solar water heater. *Solar Energy*, 82(7), 602–612. doi: 10.1016/j.solener.2008.02.005

[3] Kandlikar, S.G. (2002). Fundamental issues related to flow boiling in minichannels and microchannels. *Experimental Thermal and Fluid Science*, 26(2–4), 389–407. doi: 10.1016/S0894-1777(02)00150-4

[4] Lu, K., Wang, C., Wang, C., Fan, X., Qi, F., & He, H. (2023). Topological structures for microchannel heat sink applications – a review. *Manufacturing Review*, 10(2). doi: 10.1051/mfreview/2022035

[5] Harirchian, T., & Garimella, S.V. (2009). Effects of channel dimension, heat flux, and mass flux on flow boiling regimes in microchannels. *International Journal of Multiphase Flow*, 35(4), 349–362. doi: 10.1016/j.ijmultiphaseflow.2009.01.003

[6] Mihai, I.C. (2009). Heat transfer in minichannels and microchannels CPU cooling systems. *Advanced Topics in Optoelectronics, Microelectronics, and Nanotechnologies* IV, 72971N, 7 Jan. Constanta, Romania. doi: 10.1117/12.823670

[7] Prończuk, M., & Krzanowska. A. (2021). Experimental investigation of the heat transfer and pressure drop inside tubes and the shell of a minichannel shell and tube type heat exchanger. *Energies*, 14(24). doi: 10.3390/en14248563

[8] Lan, Y., Feng, Z., Hu, Z., Zheng, S., Zhou, J., Zhang, Y., Huang, Z., Zhang, J., & Lu, W. (2023). Experimental investigation on the effects of swirling flow on flow boiling heat transfer and instability in a minichannel heat sink. *Applied Thermal Engineering*, 219(B), 119512. doi: 10.1016/j.applthermaleng.2022.119512

[9] Ye, H., Zhao, H., Yong, L., Lum, X., & Yao, J. (2025). Unveiling flow boiling hysteresis mechanisms and characteristics of R134a within minichannels. *International Journal of Heat and Mass Transfer*, 249, 127244. doi: 10.1016/j.ijheatmasstransfer.2025.127244

[10] Yaghoubi, M.S., Ahmadpour, A., & Saffar-Avval, M. (2025). Geometrical design of minichannels with rectangular wall cavities for flow boiling heat transfer enhancement. *Results in Engineering*, 25, 103989. doi: 10.1016/j.rineng.2025.103989

[11] Ye, H., Lum, L.Y.X., Kandasamy, R., Zhao, H., & Ho, J.Y. (2024). Flow boiling heat transfer enhancement of R134a in additively manufactured minichannels with microengineered surfaces. *Applied Thermal Engineering*, 256, 124150. doi: 10.1016/j.applthermaleng.2024.124150

[12] Shang, H., Xia, G., Li, R., & Miao, S. (2025). Experimental study on flow boiling heat transfer of HFE-7100 in minichannel heat sinks for professional-grade server chips cooling. *International Communications in Heat and Mass Transfer*, 164(A), 108825. doi: 10.1016/j.icheatmasstransfer.2025.108825

[13] Sun, J., Lin, Y., Li, J., Tang, W., Li, W., Ahmad, W., & Zhao, J. (2024). Heat transfer and visualization of flow boiling on nanowire surfaces in the microchannel. *Applied Thermal Engineering*, 256, 124064, doi: 10.1016/j.applthermaleng.2024.124064.

[14] Li, T., Luo, X., & Li, G. (2024). Instability analysis of pressure drop and flow characteristics in mini-channel heat sink with phase-separated configuration. *Applied Thermal Engi*neering, 253, 123755. doi: 10.1016/j.applthermaleng.2024.123755

[15] Hsu, H.Y., Kumar, R., & Lin, C.W. (2024). A numerical investigation of the wettability effect on minitube flow boiling using the volume of fluid method. *International Journal of Heat and Mass Transfer*, 225, 125370. doi: 10.1016/j.ijheatmasstransfer.2024.125370

[16] Pereira, J.E., Souza, R.R., & Moita, A.S. (2026). Experimental factors and techniques for pool boiling heat transfer enhancement: A critical review. *Heat Transfer*, 55(4), 2201–2232. doi: 10.1002/ htj.70197

[17] Etminan, A. Muzychka, Y.S., & Pope, K. (2021). A review on the hydrodynamics of Taylor flow in microchannels: Experimental and computational st*udies*. *Processe*s, 9(5), 870. doi: 10.3390/pr9050870

[18] Piasecka, M., Hożejowska, S., Pawińska, A., & Strąk, D. (2022). Heat transfer analysis of a co-current heat exchanger with two rectangular mini-channels. *Energie*s, 15(4), 1340. doi: 10.3390/en15041340

[19] Strąk, K., & Strąk, D. (2025). Experimental analysis of heat transfer in multi-mini-channel module: A comparison with CFD simulations. *Energies*, 18(22), 5992. doi:10.3390/en18225992

[20] Strąk, D., Hożejowska, S., Pawińska, A., & Piasecka, M. (2022). Research on a flow heat exchanger with minichannels. In *Advances in heat and mass transfer studies*. *Proceedings of the 16th Symposium on Heat and Mass Transfe*r (276−286). Oficyna Wydawnicza Politechniki Białostockiej, Białystok (in Polish). doi: 10.24427/978-83-67185-30-1_29

[21] Strąk, D. (2023). Performance investigation of hybrid photovoltaic thermal-heat with mini-channels for application in electric vehicles. *The Archives of Automotive Engineering – Archiwum Motoryzacji*, 100(2), 1–26. doi: 10.14669/AM/166810

[22] Mahmood, H., Freegah, B., Faik, A.M.El-D., & Saleh, Q. (2025). Optimizing minichannel heat sink design: A combined numerical and experimental analysis of inlet/outlet configurations and pin fin enhancements. *Heat Transfer*, 54(3), 1921–1939. doi: 10.1002/htj.23267

[23] Mozafari, M., Lee, A., & Mohammadpour, J. (2021). Thermal management of single and multiple PCMs based heat sinks for electronics cooling. *Thermal Science and Engineering Progress*, 23, 100919. doi: 10.1016/j.tsep.2021.100919

[24] Mahmood, H., & Freegah, B. (2026). Optimizing fluid flow to enhance the hydrothermal performance of multi-mini-channel heat sinks. *Heat Transfer*, 55(2), 1071–1082. doi: 10.1002/htj.70122

[25] Strąk, D., Piasecka, M., Pawińska, A., & Hożejowska, S. (2020). Investigation of heat transfer during flow through minichannels of a compact heat exchanger. In *Contemporary Issues in Thermodynamics* (181−190). *The 24th Congress of Thermodynamicists*, 27-30 Oct., Białobrzegi, Poland. Oficyna Wydawnicza Politechniki Warszawskiej (in Polish).

[26] Madejski, J. (1998). *Theory of heat transfer*. Wydawnictwo Politechniki Szczecińskiej, Szczecin (in Polish).

[27] Tran, T.N., Wambsganss, M.W., & France, D.M. (1996). Small circular- and rectangular-channel boiling with two refrigerants. *International Journal of Multiphase Flow*, 22(3) 485–498. doi: 10.1016/0301-9322(96)00002-X

[28] Olmeda, P., Margot, X., García-Tíscar, J., & Kumar, K. (2026). Numerical and experimental analysis of mini cooling channel flow dynamics. *Journal of the Brazilian Society of Mechanical Sciences and Engineering*, 48(3), 194. doi:10.1007/s40430-025-06161-0